Time-correlation functions in molecular liquids studied by the mode-coupling theory based on the interaction-site model

Song-Ho Chong[1] and Fumio Hirata[2,*]
[1]*Department of Chemistry, Graduate School of Science, Kyoto University, Kyoto 606-8502, Japan*
[2]*Institute for Molecular Science, Myodaiji, Okazaki, Aichi, 444-8585, Japan*
(Received 10 June 1998)

Numerical results for longitudinal current spectra, velocity autocorrelation functions, and diffusion coefficients of a model diatomic liquid are presented using the recently developed theory for dynamics of classical polyatomic fluids. The theory is based on the interaction-site model for molecular liquids, the projection-operator formalism, and mode-coupling theory. The effect of the inclusion of a slow contribution in memory kernels, represented by the mode-coupling expression, on the aforementioned dynamical quantities is discussed. A molecular dynamics simulation of the same system is also performed to test the accuracy of our theory, and the theoretical results are found to be in fair agreement with those obtained from the simulation. [S1063-651X(98)01412-3]

PACS number(s): 61.20.Lc, 61.25.Em

I. INTRODUCTION

In two recent papers [1,2] (hereafter referred to as papers I and II, respectively), we developed a microscopic theory for the dynamics of polyatomic fluids based on the projection-operator formalism of Zwanzig and Mori [3–5], and on the interaction-site model for molecular liquids [6,7]. In paper I, an approximation scheme was developed for memory functions appearing in the generalized Langevin equation by assuming an exponential form for the memory functions, and by extending the method of Lovesey and coworkers for monatomic liquids [8,9] to polyatomic fluids. The resulting theory was applied to calculations of space-time density correlation functions and longitudinal current spectra, and was shown to provide a rather satisfactory account of the main features of collective excitations in classical molecular liquids.

However, an intense investigation through theoretical, experimental, and molecular dynamics simulation studies for simple liquids has revealed that the microscopic processes underlying various time-dependent phenomena cannot be fully accounted for by a simplified memory-function approach [10–12]. In particular, the assumption that the decay of the memory functions is ruled by a simple exponential-type relaxation must be significantly revised in view of the results of the kinetic framework developed for dense simple liquids [13–21]. This motivated us to improve the theory further for the dynamics of polyatomic fluids: this work was presented in paper II.

The central idea adopted in paper II was borrowed from the works of Sjögren [20,21], and was to separate the memory functions into a fast portion arising from rapidly decaying ''binary collision'' contributions, and a slow portion which stems from correlated collisional effects. In paper II, the fast portion of the memory functions was obtained by exploiting ''frequency sum rules,'' and, for the treatment of the slow portion, we developed a mode-coupling theory for molecular liquids based on the interaction-site model.

The resulting theory in paper II provides closed nonlinear equations for a self-consistent treatment of density propagation in a classical polyatomic fluid. This paper presents numerical results for longitudinal current spectra, velocity autocorrelation functions, and diffusion coefficients of a model diatomic liquid based on this theory, and a consequence of the inclusion of the slow portion in the memory functions is discussed. The site-site static structure factors and direct correlation functions, which are required as input in our theory for dynamics, are obtained from an integral equation theory conventionally referred to as ex-RISM (the extended version of the reference interaction-site method) [22,23]. To test the accuracy of the theory, a molecular dynamics simulation of the same system is also performed, and the theoretical results are compared with those obtained from the simulation.

II. THEORY

In this section, we briefly outline the theory for dynamics of molecular liquids that is needed in our theoretical calculations. For their derivation, we refer to papers I and II. A theory for velocity correlation functions and diffusion coefficients of polyatomic fluids is also presented. Throughout this section, we consider a homogeneous and isotropic fluid composed of N rigid molecules in a volume V at the inverse temperature $\beta=1/k_BT$, and the thermodynamic limit with density $\rho=N/V$ is implied.

A. Basic definitions

We begin with the definition of two basic dynamical variables $\boldsymbol{\delta\rho}$ and $\mathbf{j}$. $\boldsymbol{\delta\rho}$ and $\mathbf{j}$ are row vectors whose components are, respectively, a local density and a longitudinal current density of atom (site) α at time t in Fourier k space:

$$\delta\rho_\alpha(\mathbf{k},t)\equiv\sum_i e^{i\mathbf{k}\cdot\mathbf{r}_i^\alpha(t)}, \tag{1}$$

*Author to whom correspondence should be addressed. FAX: +81 564 53 4660. Electronic address: hirata@ims.ac.jp

$$j_\alpha(\mathbf{k},t)\equiv\sum_i v_{i,z}^\alpha(t)e^{i\mathbf{k}\cdot\mathbf{r}_i^\alpha(t)}, \tag{2}$$

where $\mathbf{r}_i^\alpha(t)$ and $v_{i,z}^\alpha(t)$ denote the location and the z-component velocity of atom α in the ith molecular at time t, respectively, and the wave vector $\mathbf{k}$ is chosen such that it is along the z axis of the space-fixed laboratory frame. Hereafter, the Greek subscripts and superscripts refer to the interaction sites of a molecule, and the Roman letters label the molecules unless specified otherwise. These two densities satisfy the continuity equation

$$\dot{\delta}\rho_\alpha(\mathbf{k},t)=ikj_\alpha(\mathbf{k},t), \tag{3}$$

where the dot denotes the time derivative.

The matrices of the site-site intermediate scattering functions and the longitudinal current correlation functions are defined, respectively, by

$$\mathbf{F}(k,t)\equiv(\boldsymbol{\delta\rho}(\mathbf{k}),\boldsymbol{\delta\rho}(\mathbf{k},t)), \tag{4}$$

$$\mathbf{J}(k,t)\equiv(\mathbf{j}(\mathbf{k}),\mathbf{j}(\mathbf{k},t)). \tag{5}$$

(The absence of any indication for time t in a dynamical variable means that the latter is evaluated at $t=0$.) Here the inner product of two row vectors, $\mathbf{A}_1$ and $\mathbf{A}_2$, is defined as the canonical ensemble average

$$(\mathbf{A}_1,\mathbf{A}_2)\equiv\frac{1}{N}\langle\mathbf{A}_1^\dagger\mathbf{A}_2\rangle, \tag{6}$$

where $\mathbf{A}_1^\dagger$ denotes a column vector adjoint to $\mathbf{A}_1$, and the factor $1/N$ is a matter of convention.

The initial value of $\mathbf{F}(k,t)$ is the matrix of the site-site static structure factors

$$\mathbf{F}(k,0)\equiv\boldsymbol{\chi}(k)=\mathbf{w}(k)+\rho\mathbf{h}(k), \tag{7}$$

where $\mathbf{w}(k)$ and $\mathbf{h}(k)$ are the intramolecular and intermolecular total correlation function matrices defined by

$$w_{\alpha\beta}(k)\equiv\frac{1}{N}\left\langle\sum_i e^{-i\mathbf{k}\cdot\mathbf{r}_i^\alpha}e^{i\mathbf{k}\cdot\mathbf{r}_i^\beta}\right\rangle, \tag{8}$$

$$\rho h_{\alpha\beta}(k)\equiv\frac{1}{N}\left\langle\sum_i\sum_{j\neq i}e^{-i\mathbf{k}\cdot\mathbf{r}_i^\alpha}e^{i\mathbf{k}\cdot\mathbf{r}_j^\beta}\right\rangle. \tag{9}$$

Having assumed a molecule to be rigid, $w_{\alpha\beta}(k)$ is given by

$$w_{\alpha\beta}(k)=\delta_{\alpha\beta}+(1-\delta_{\alpha\beta})j_0(kl_{\alpha\beta}), \tag{10}$$

in which $j_0(x)$ is the zeroth-order spherical Bessel function, and $l_{\alpha\beta}$ denotes the ''bond'' length between α and β sites.

The initial value of $\mathbf{J}(k,t)$ for a rigid molecule generically consists of its translational and rotational contributions,

$$\mathbf{J}(k,0)\equiv\mathbf{J}(k)=\mathbf{J}^{\mathrm{trans}}(k)+\mathbf{J}^{\mathrm{rot}}(k), \tag{11}$$

and can be expressed in terms of inertia parameters such as total mass and principal moment of inertia of the molecule. Explicit expressions for the elements of $\mathbf{J}(k)$ for a water molecule [24,25] and a diatomic molecule [1] can be found elsewhere.

The matrices of the site-site dynamic structure factors and the longitudinal current spectra are defined, respectively, as the time Fourier transforms of the corresponding time-correlation function matrices:

$$\mathbf{S}(k,\omega)\equiv\int_{-\infty}^{\infty}dt\,e^{i\omega t}\mathbf{F}(k,t), \tag{12}$$

$$\mathbf{C}_L(k,\omega)\equiv\int_{-\infty}^{\infty}dt\,e^{i\omega t}\mathbf{J}(k,t). \tag{13}$$

The continuity equation [Eq. (3)], implies that these two matrices are connected through the relation

$$\mathbf{C}_L(k,\omega)=\frac{\omega^2}{k^2}\mathbf{S}(k,\omega). \tag{14}$$

We define here for later convenience the unnormalized and normalized nth frequency moment matrices of $\mathbf{S}(k,\omega)$:

$$\overline{\boldsymbol{\omega}_k^n}\equiv\frac{1}{2\pi}\int_{-\infty}^{\infty}d\omega\,\omega^n\mathbf{S}(k,\omega)=(-1)^{n/2}\left[\frac{d^n}{dt^n}\mathbf{F}(k,t)\right]_{t=0}, \tag{15}$$

$$\langle\boldsymbol{\omega}_k^n\rangle\equiv\overline{\boldsymbol{\omega}_k^n}\left[\frac{1}{2\pi}\int_{-\infty}^{\infty}d\omega\,\mathbf{S}(k,\omega)\right]^{-1}=\overline{\boldsymbol{\omega}_k^n}\boldsymbol{\chi}^{-1}(k), \tag{16}$$

where we have used Eq. (7) and the inverse relation of Eq. (12).

We next consider single-particle counterparts. The term ''particle'' in this paper refers to one molecule as a whole, and not to an individual atom which constitutes the molecule. Our basic dynamical variables in this case are density and longitudinal current density of an arbitrarily chosen tagged particle, $\boldsymbol{\delta\rho}^s$ and $\mathbf{j}^s$, whose components are given, respectively, by

$$\delta\rho_\alpha^s(\mathbf{k},t)=e^{i\mathbf{k}\cdot\mathbf{r}_1^\alpha(t)}, \tag{17}$$

$$j_\alpha^s(\mathbf{k},t)=v_{1,z}^\alpha(t)e^{i\mathbf{k}\cdot\mathbf{r}_1^\alpha(t)}. \tag{18}$$

The self parts of $\mathbf{F}(k,t)$ and $\mathbf{J}(k,t)$ are defined, respectively, by

$$\mathbf{F}^s(k,t)\equiv(\boldsymbol{\delta\rho}^s(\mathbf{k}),\boldsymbol{\delta\rho}^s(\mathbf{k},t))_s, \tag{19}$$

$$\mathbf{J}^s(k,t)\equiv(\mathbf{j}^s(\mathbf{k}),\mathbf{j}^s(\mathbf{k},t))_s, \tag{20}$$

where the inner product in the single-particle variable case is given by

$$(\mathbf{A}_1^s,\mathbf{A}_2^s)_s\equiv\langle\mathbf{A}_1^{s\dagger}\mathbf{A}_2^s\rangle. \tag{21}$$

Note the absence of the factor of $1/N$ compared to Eq. (6). The initial value of $\mathbf{F}^s(k,t)$ reads [see Eq. (8)]

$$\mathbf{F}^s(k,0)=\mathbf{w}(k), \tag{22}$$

whereas that of $\mathbf{J}^s(k,t)$ is given by

$$\mathbf{J}^s(k,0)=\mathbf{J}(k). \tag{23}$$

The appearance of $\mathbf{J}(k)$, which is common to the collective variable case [see Eq. (11)], is due to the fact that $\mathbf{J}(k)$ is essentially a single-particle quantity, since the velocities of different molecules at the same time are statistically independent.

The self parts of $\mathbf{S}(k,\omega)$ and $\mathbf{C}_L(k,\omega)$ are defined as the time Fourier transforms of $\mathbf{F}^s(k,t)$ and $\mathbf{J}^s(k,t)$, respectively. The unnormalized and normalized frequency moment matrices of $\mathbf{S}^s(k,\omega)$ are also defined as in Eqs. (15) and (16):

$$\overline{\boldsymbol{\omega}_{k,s}^n} \equiv \frac{1}{2\pi}\int_{-\infty}^{\infty} d\omega\, \omega^n \mathbf{S}^s(k,\omega) = (-1)^{n/2}\left[\frac{d^n}{dt^n}\mathbf{F}^s(k,t)\right]_{t=0}, \tag{24}$$

$$\langle \boldsymbol{\omega}_{k,s}^n \rangle \equiv \overline{\boldsymbol{\omega}_{k,s}^n}\left[\frac{1}{2\pi}\int_{-\infty}^{\infty} d\omega\, \mathbf{S}^s(k,\omega)\right]^{-1} = \overline{\boldsymbol{\omega}_{k,s}^n}\mathbf{w}^{-1}(k). \tag{25}$$

B. Collective dynamics

The time-evolution equation for $\mathbf{F}(k,t)$ is given by the generalized Langevin equation (GLE) [1,2]

$$\ddot{\mathbf{F}}(k,t) + \langle \boldsymbol{\omega}_k^2 \rangle \mathbf{F}(k,t) + \int_0^t d\tau\, \mathbf{K}(k,t-\tau)\dot{\mathbf{F}}(k,\tau) = \mathbf{0}, \tag{26}$$

where $\langle \boldsymbol{\omega}_k^2 \rangle$ denotes the normalized second frequency moment matrix of $\mathbf{S}(k,\omega)$ defined by Eq. (16), and is given by

$$\langle \boldsymbol{\omega}_k^2 \rangle = k^2 \mathbf{J}(k)\boldsymbol{\chi}^{-1}(k). \tag{27}$$

$\mathbf{K}(k,t)$ in Eq. (26) is the memory function matrix (or simply called the memory kernel), for which two different approximation schemes were developed in papers I and II. In the present work, we adopt an approximation scheme based on the mode-coupling theory described in paper II, and write $\mathbf{K}(k,t)$ in the form

$$\mathbf{K}(k,t) = \mathbf{K}_{\text{fast}}(k,t) + \mathbf{K}_{\text{slow}}(k,t). \tag{28}$$

$\mathbf{K}_{\text{fast}}(k,t)$ denotes the fast portion of the memory kernel which is due to the rapidly decaying binary collision contributions (associated with fast collisional events), and is given by [2]

$$\mathbf{K}_{\text{fast}}(k,t) = \mathbf{U}(k)\{\text{diag}[g(t/\tau_\alpha(k))]\}\mathbf{U}^{-1}(k)\mathbf{K}(k,0). \tag{29}$$

In this equation, $\tau_\alpha^{-2}(k)$'s denote eigenvalues of the matrix $\boldsymbol{\tau}^{-2}(k)$ defined through

$$\boldsymbol{\tau}^{-2}(k) \equiv -\frac{1}{2}\ddot{\mathbf{K}}(k,0)\mathbf{K}^{-1}(k,0), \tag{30}$$

$$\mathbf{K}(k,0) = \langle \boldsymbol{\omega}_k^4 \rangle \langle \boldsymbol{\omega}_k^2 \rangle^{-1} - \langle \boldsymbol{\omega}_k^2 \rangle, \tag{31}$$

$$-\ddot{\mathbf{K}}(k,0) = \langle \boldsymbol{\omega}_k^6 \rangle \langle \boldsymbol{\omega}_k^2 \rangle^{-1} - (\langle \boldsymbol{\omega}_k^4 \rangle \langle \boldsymbol{\omega}_k^2 \rangle^{-1})^2, \tag{32}$$

in terms of the normalized frequency moments of $\mathbf{S}(k,\omega)$ defined in Eq. (16), and $\mathbf{U}(k)$ is a matrix which diagonalizes $\boldsymbol{\tau}^{-2}(k)$. $g(x)$ is a shape function which decays rapidly and satisfies $g(x) \approx 1 - x^2$ for small x, and diag( ) represents a diagonal matrix. In the present paper, we employ the shape function $g(x) = \text{sech}^2(x)$.

$\mathbf{K}_{\text{slow}}(k,t)$ in Eq. (28) denotes the slow portion of the memory kernel which stems from correlated collisional effects, whose expression under the mode-coupling theory reads [2]

$$\begin{aligned}[K_{\text{slow}}(k,t)]_{\alpha\beta} &= \frac{\rho}{(2\pi)^3}\sum_{\lambda,\mu,\nu}\int d\mathbf{q}\{q_z^2[wc(q)]_{\lambda\mu}[wc(q)]_{\beta\nu} \\ &\times (1 - f_{\mu\nu}(q,t)f_{\lambda\beta}(k-q,t))F_{\mu\nu}(q,t)F_{\lambda\beta}(k-q,t) \\ &+ q_z(k-q_z)[wc(q)]_{\lambda\mu}[wc(k-q)]_{\beta\nu} \\ &\times (1 - f_{\mu\beta}(q,t)f_{\lambda\nu}(k-q,t)) \\ &\times F_{\mu\beta}(q,t)F_{\lambda\nu}(k-q,t)\}J_{\alpha\lambda}(k).\end{aligned} \tag{33}$$

The main assumption and approximations used to derive the above mode coupling expression are (i) to assume that the slow decay of the memory kernel at long times is due to the couplings to wave-vector-dependent density modes of the form $\delta\rho_\lambda(\mathbf{q})\,\delta\rho_\mu(\mathbf{p})$, (ii) to decouple (or factorize) the four-site correlation functions into two-site ones, and (iii) to use the convolution approximation for three-site correlation functions [2]. The last approximation for molecular liquids is a generalization of those which have been successful in the mode-coupling theory for simple liquids [12,26,27].

In Eq. (33), $[wc(k)]_{\alpha\beta}$ is defined by

$$[wc(k)]_{\alpha\beta} \equiv \sum_\gamma w_{\alpha\gamma}(k)c_{\gamma\beta}(k), \tag{34}$$

where $c_{\alpha\beta}(k)$ denotes the site-site direct correlation function, and $f_{\alpha\beta}(k,t)$ is an auxiliary function defined by

$$f_{\alpha\beta}(k,t) \equiv \frac{F_{\alpha\beta}^0(k,t)}{F_{\alpha\beta}^s(k,t)}, \tag{35}$$

where $F_{\alpha\beta}^0(k,t)$ denotes an element of the following intermediate scattering function matrix:

$$\mathbf{F}^0(k,t) \equiv \exp[-\tfrac{1}{2}\langle \boldsymbol{\omega}_{k,s}^2 \rangle t^2]\mathbf{w}(k). \tag{36}$$

This auxiliary function is required to guarantee that $\mathbf{K}_{\text{slow}}(k,t)$ evolves at the order of t^4 in the short-time regime discussed in paper II. Numerical results for $\mathbf{F}(k,t)$ can be obtained self-consistently based on Eqs. (26), (28), (29), and (33) (see also Sec. III B).

C. Single-particle dynamics

The single-particle counterpart of Eq. (26) is given by

$$\ddot{\mathbf{F}}^s(k,t) + \langle \boldsymbol{\omega}_{k,s}^2 \rangle \mathbf{F}^s(k,t) + \int_0^t d\tau\, \mathbf{K}^s(k,t-\tau)\dot{\mathbf{F}}^s(k,\tau) = \mathbf{0}, \tag{37}$$

in which

$$\langle \boldsymbol{\omega}_{k,s}^2 \rangle = k^2 \mathbf{J}(k) \mathbf{w}^{-1}(k). \tag{38}$$

$\mathbf{K}^s(k,t)$ is the memory kernel in the single-particle variable case, and it also consists of its fast and slow portions:

$$\mathbf{K}^s(k,t) = \mathbf{K}^s_{\rm fast}(k,t) + \mathbf{K}^s_{\rm slow}(k,t). \tag{39}$$

The fast portion of the memory kernel $\mathbf{K}^s(k,t)$ is given by [2]

$$\mathbf{K}^s_{\rm fast}(k,t) = \mathbf{U}_s(k)\{\mathrm{diag}[g(t/\tau_{s,\alpha}(k))]\}\mathbf{U}_s^{-1}(k)\mathbf{K}^s(k,0), \tag{40}$$

where $\tau_{s,\alpha}^{-2}(k)$'s are the eigenvalues of the matrix $\boldsymbol{\tau}_s^{-2}(k)$ defined by

$$\boldsymbol{\tau}_s^{-2}(k) \equiv -\tfrac{1}{2}\ddot{\mathbf{K}}^s(k,0)[\mathbf{K}^s(k,0)]^{-1}, \tag{41}$$

and $\mathbf{U}_s(k)$ is a matrix which diagonalizes $\boldsymbol{\tau}_s^{-2}(k)$. The matrices appearing in the right-hand side of Eq. (41) can be expressed, as in Eqs. (31) and (32), as

$$\mathbf{K}^s(k,0) = \langle \boldsymbol{\omega}_{k,s}^4 \rangle \langle \boldsymbol{\omega}_{k,s}^2 \rangle^{-1} - \langle \boldsymbol{\omega}_{k,s}^2 \rangle, \tag{42}$$

$$-\ddot{\mathbf{K}}^s(k,0) = \langle \boldsymbol{\omega}_{k,s}^6 \rangle \langle \boldsymbol{\omega}_{k,s}^2 \rangle^{-1} - (\langle \boldsymbol{\omega}_{k,s}^4 \rangle \langle \boldsymbol{\omega}_{k,s}^2 \rangle^{-1})^2 \tag{43}$$

in terms of the normalized frequency moment matrices of $\mathbf{S}^s(k,\omega)$ defined in Eq. (25). The expression for $\mathbf{K}^s_{\rm slow}(k,t)$ under the mode-coupling theory reads [2]

$$[K^s_{\rm slow}(k,t)]_{\alpha\beta} = \frac{\rho}{(2\pi)^3} \sum_{\lambda,\mu,\nu} \int d\mathbf{q}(k-q_z)^2 [wc(k-q)]_{\lambda\mu} [wc(k-q)]_{\beta\nu} (1 - f_{\lambda\beta}(q,t) f_{\mu\nu}(k-q,t)) \times F^s_{\lambda\beta}(q,t) F_{\mu\nu}(k-q,t) J_{\alpha\lambda}(k). \tag{44}$$

Numerical results for the single particle $\mathbf{F}^s(k,t)$ can be obtained based on Eqs. (37), (39), (40), and (44) (see also Sec. III B).

D. Velocity correlation functions

In this subsection, we derive a time-evolution equation for site-site velocity correlation functions defined by

$$Z_{\alpha\beta}(t) \equiv \langle v_\alpha(0) v_\beta(t) \rangle, \tag{45}$$

where α and β sites belong to the same molecule. [That is, $Z_{\alpha\beta}(t)$ is a single-particle quantity.] It is obvious in view of Eq. (20) that $Z_{\alpha\beta}(t)$ is also given by

$$Z_{\alpha\beta}(t) = \lim_{k\to 0} J^s_{\alpha\beta}(k,t). \tag{46}$$

To obtain the equation for $Z_{\alpha\beta}(t)$, we start from the continued-fraction representation ($\mathbf{I}$ being the unit matrix)

$$\begin{aligned} \tilde{\mathbf{F}}^s(k,z)\mathbf{w}^{-1}(k) &= -[z\mathbf{I} + \tilde{\mathbf{M}}^s(k,z)]^{-1} \\ &= -\{z\mathbf{I} - [z\mathbf{I} + \tilde{\mathbf{K}}^s(k,z)]^{-1} \langle \boldsymbol{\omega}_{k,s}^2 \rangle\}^{-1}, \end{aligned} \tag{47}$$

where the Laplace transform of $\mathbf{F}^s(k,t)$ is defined by

$$\tilde{\mathbf{F}}^s(k,z) \equiv i \int_0^\infty dt\, e^{izt} \mathbf{F}^s(k,t) \quad (\mathrm{Im}\, z > 0). \tag{48}$$

$\tilde{\mathbf{M}}^s(k,z)$ and $\tilde{\mathbf{K}}^s(k,z)$, respectively, are the Laplace transforms of the first- and second-order memory function matrices of $\mathbf{F}^s(k,t)$. We notice that the second-order memory kernel $\mathbf{K}^s(k,t)$ is defined from an operator which projects any variable onto the subspace spanned by $\boldsymbol{\delta\rho}^s(\mathbf{k})$ and $\mathbf{j}^s(\mathbf{k})$ [1,2], and the second equality of Eq. (47) follows by Laplace transforming Eq. (37). On the other hand, the first-order memory kernel $\mathbf{M}^s(k,t)$ is derived from an operator which projects any variable $\mathbf{X}(\mathbf{k})$ onto the subspace spanned by $\boldsymbol{\delta\rho}^s(\mathbf{k})$:

$$\mathcal{P}\mathbf{X}(\mathbf{k}) = \boldsymbol{\delta\rho}^s(\mathbf{k}) (\boldsymbol{\delta\rho}^s(\mathbf{k}), \boldsymbol{\delta\rho}^s(\mathbf{k}))_s^{-1} (\boldsymbol{\delta\rho}^s(\mathbf{k}), \mathbf{X}(\mathbf{k}))_s. \tag{49}$$

A standard procedure of the projection operator formalism leads to [10–12]

$$\begin{aligned} \mathbf{M}^s(k,t) &= (\dot{\boldsymbol{\delta\rho}}^s(\mathbf{k}), \exp(i\mathcal{Q}\mathcal{L}t)\, \dot{\boldsymbol{\delta\rho}}^s(\mathbf{k}))_s \mathbf{w}^{-1}(k) \\ &= k^2 (\mathbf{j}^s(\mathbf{k}), \exp(i\mathcal{Q}\mathcal{L}t)\mathbf{j}^s(\mathbf{k}))_s \mathbf{w}^{-1}(k), \end{aligned} \tag{50}$$

where $\mathcal{Q} = 1 - \mathcal{P}$, and in the second equality we used the continuity equation. Since it is exact to replace the anomalous time-propagator $\exp(i\mathcal{Q}\mathcal{L}t)$ by the conventional one, $\exp(i\mathcal{L}t)$, in the $k \to 0$ limit [12] one finds [see Eq. (20)]

$$\lim_{k\to 0} \mathbf{M}^s(k,t) = k^2 \mathbf{J}^s(k,t) \mathbf{w}^{-1}(k). \tag{51}$$

From Eq. (47), the Laplace transform of the time-evolution equation for $\mathbf{M}^s(k,t)$ reads

$$\tilde{\mathbf{M}}^s(k,z) = -[z\mathbf{I} + \tilde{\mathbf{K}}^s(k,z)]^{-1} \langle \boldsymbol{\omega}_{k,s}^2 \rangle, \tag{52}$$

where one should notice that $\mathbf{M}^2(k,0) = \langle \boldsymbol{\omega}_{k,s}^2 \rangle$. Using Eqs. (38), (46), and (51), this equation can be rearranged into the Laplace transformed equation for $\mathbf{Z}(t)$:

$$\tilde{\mathbf{Z}}(z) = -[z\mathbf{I} + \tilde{\mathbf{K}}^s(z)]^{-1} \mathbf{Z}(0), \tag{53}$$

where $\tilde{\mathbf{K}}^s(z)$ denotes the Laplace transform of

$$\mathbf{K}^s(t) \equiv \lim_{k\to 0} \mathbf{K}^s(k,t). \tag{54}$$

Laplace inverting Eq. (53) finally yields the GLE for $\mathbf{Z}(t)$:

$$\dot{\mathbf{Z}}(t) = -\int_0^t d\tau\, \mathbf{K}^s(t-\tau)\mathbf{Z}(\tau), \tag{55}$$

which is a direct generalization of the well-known expression for simple liquids [10–12]. Thus, the site-site velocity correlation functions can be obtained based on the knowledge of the memory kernel, $\mathbf{K}^s(k,t)$.

E. Diffusion coefficients

We next investigate diffusion coefficients of molecular liquids. In contrast to the monatomic liquid case, diffusion coefficients consist not only of the translational contribution but also of the rotational one.

To this end, let us consider the overdamped limit of Eq. (37). The overdamped limit is achieved by neglecting the inertia term $\ddot{\mathbf{F}}^s(k,t)$, and by invoking the Markovian approximation for the memory kernel [28]; the resultant expression reads

$$\langle \boldsymbol{\omega}_{k,s}^2 \rangle \mathbf{F}^s(k,t) + \boldsymbol{\xi}(k)\dot{\mathbf{F}}^s(k,t) = \mathbf{0}, \tag{56}$$

where the friction matrix $\boldsymbol{\xi}(k)$ is defined by

$$\boldsymbol{\xi}(k) = \int_0^\infty dt\, \mathbf{K}^s(k,t). \tag{57}$$

By noting Eq. (22), the solution to Eq. (56) is easily found to be

$$\mathbf{F}^s(k,t) = \exp[-\boldsymbol{\xi}^{-1}(k)\langle \boldsymbol{\omega}_{k,s}^2 \rangle t]\mathbf{w}(k) = \exp[-\mathbf{D}(k)t]\mathbf{w}(k), \tag{58}$$

where, in the second equality, we have defined the wave-vector-dependent diffusion-coefficient matrix

$$\mathbf{D}(k) = \boldsymbol{\xi}^{-1}(k)\langle \boldsymbol{\omega}_{k,s}^2 \rangle. \tag{59}$$

A more useful and physically clearer expression for $\mathbf{D}(k)$ can be obtained in terms of the velocity correlation functions as follows. By taking the $z\to 0$ limit of Eq. (52), one finds [see Eq. (48)]

$$\mathbf{D}(k) = \int_0^\infty dt\, \mathbf{M}^s(k,t). \tag{60}$$

Using Eq. (51), it follows, in the small-k region, that

$$\mathbf{D}(k) = k^2 \int_0^\infty dt\, \mathbf{J}^s(k,t)\mathbf{w}^{-1}(k) \quad (\text{as } k\to 0+). \tag{61}$$

In view of Eq. (46), this equation essentially expresses the diffusion-coefficient matrix as the time integral of the site-site velocity correlation functions. Thus, Eq. (61) can be regarded as a generalization of the well-known Green-Kubo formula for the translational diffusion coefficient of simple liquids, which in our notation reads

$$D(k) = k^2 \int_0^\infty dt \langle v_z(0)v_z(t)\rangle. \tag{62}$$

In the case of molecular liquids, the rotational motion as well as the translational one contributes to $\mathbf{D}(k)$, and the resulting $\mathbf{D}(k)$ reflects both kinds of motions. As will be discussed in Sec. IV C, the translational and rotational contributions can be extracted by diagonalizing the matrix $\mathbf{D}(k)$. In the present paper, we consider a liquid consisting of diatomic molecules (see Sec. IV A), and $\mathbf{D}(k)$ is given by a 2×2 matrix. One therefore obtains two eigenvalues by diagonalizing $\mathbf{D}(k)$. An eigenvalue of $\mathbf{D}(k)$ related to the translational motion should vary as k^2 in the small-k regime [see Eq. (62)], whereas that related to the rotational motion should remain finite in the $k\to 0$ limit [11]. Thus, if we denote the translational and rotational diffusion coefficients as D^T and D^R, respectively, one can expect the eigenvalues of $\mathbf{D}(k)$ [$\boldsymbol{D}(k)_E$] to behave as

$$\boldsymbol{D}(k)_E \to k^2 D^T, D^R \quad (\text{as } k\to 0+). \tag{63}$$

We will see later that the behavior represented by Eq. (63) is indeed observed in our model liquid, and further discussion concerning the diffusion coefficients will be made in Sec. IV C. Finally, it should be noted that, although $\mathbf{w}^{-1}(k)$ is singular in the $k\to 0$ limit [see Eq. (10)], Eq. (61) as a whole is not singular owing to the presence of the factor k^2, and the $k\to 0$ limit of $\mathbf{D}(k)$ is well defined.

III. COMPUTATIONAL DETAILS

A. Treatment of the fast portion of the memory kernels

Formal expressions for the fast portion of the memory kernels are given in Eqs. (29) and (40) for the collective and single-particle variable cases, respectively, for which frequency moment matrices of $\mathbf{S}(k,\omega)$ and $\mathbf{S}^s(k,\omega)$ up to the sixth order are required. For the liquid model we consider in the present paper (see Sec. IV A), however, explicit expressions were derived in paper I for frequency moment matrices only up to the fourth order. It is of course possible to obtain the sixth-order frequency moment matrices by the same procedure as adopted in paper I, but the task is too demanding.

Alternatively, we shall proceed as follows. [For brevity, only the argument for the fast portion of the collective $\mathbf{K}(k,t)$ will be presented.] In paper I, the relaxation times for memory kernels are obtained by extending the procedure proposed by Lovesey and co-workers [8,9] to molecular fluids, which only requires the knowledge of the frequency moment matrices up to the fourth order:

$$\tau_\alpha^{-1}(k) = \xi_\alpha \sqrt{\Delta_\alpha(k)}, \tag{64}$$

where $\Delta_\alpha(k)$'s denote eigenvalues of the matrix $\boldsymbol{\Delta}(k)$ defined by

$$\boldsymbol{\Delta}(k) \equiv \langle \boldsymbol{\omega}_k^4 \rangle \langle \boldsymbol{\omega}_k^2 \rangle^{-1} - \langle \boldsymbol{\omega}_k^2 \rangle, \tag{65}$$

and ξ_α is a constant to be determined by requiring that the asymptotic form of $\tau_\alpha^{-1}(k)$ (e.g., in the $k\to\infty$ limit) satisfy a certain property. Since the relaxation times in Eq. (64) are defined in terms of the lower-order frequency moment ma-

trices, which gauge the behavior of the relevant dynamical processes in the short-time regime [see Eqs. (15) and (16)], it will be reasonable to expect that, with a certain choice of ξ_α, the relaxation times in Eq. (64) will be of the same order in magnitude as those determined from Eq. (30). Indeed, in the case of simple liquids, this expectation is rather satisfactory with a choice of $\xi_\alpha=\sqrt{3}/2$ [12]. Assuming this also to be valid in the case of molecular fluids, we approximate the fast portion of the memory kernel in Eq. (29) with $g(x)=\mathrm{sech}^2(x)$ as

$$\mathbf{K}_{\mathrm{fast}}(k,t)\approx\mathbf{U}_\Delta(k)\{\mathrm{diag}[\mathrm{sech}^2(t/\tau_\alpha(k))]\}\mathbf{U}_\Delta^{-1}(k)\mathbf{K}(k,0), \tag{66}$$

where $1/\tau_\alpha(k)$ is determined from Eq. (64) with $\xi_\alpha=\sqrt{3}/2$, and $\mathbf{U}_\Delta(k)$ is a matrix which diagonalizes $\mathbf{\Delta}(k)$. A similar construction for the fast portion of $\mathbf{K}^s(k,t)$ will also be adopted. Obviously, however, it remains to be done in the future to improve the treatment of the fast portion of the memory kernels.

B. Numerical procedure

A numerical solution of $\mathbf{F}(k,t)$ can be obtained by an iterative procedure as follows. Suppose that we have the nth approximated memory kernel $\mathbf{K}^{(n)}(k,t)$. Then, the nth approximated $\mathbf{F}^{(n)}(k,t)$ is determined via Eq. (26). When doing this, it is more conventional to work in the frequency domain and then to go back to the time domain. From Eq. (28), with Eqs. (33) and (66), one obtains the $(n+1)$th approximated memory kernel $\mathbf{K}^{(n+1)}(k,t)$ in terms of $\mathbf{F}^{(n)}(k,t)$. This procedure is continued until a certain convergence criterion is satisfied, which in the present paper is chosen to be

$$\left[\sum_{k_i=1}^{M_k}\sum_{t_j=1}^{M_t}\{K_{\alpha\beta}^{(n+1)}(k_i,t_j)-K_{\alpha\beta}^{n}(k_i,t_j)\}^2/(M_kM_t)\right]^{1/2} < 10^{-6}, \tag{67}$$

for all pairs of sites, where k_i and t_j denote spatial (in k space) and temporal grid numbers used in the numerical calculation, respectively, and M_k and M_t are the total number of grids.

We choose the initial memory kernel to be given by

$$\mathbf{K}^{(1)}(k,t)=\mathbf{K}_{\mathrm{fast}}(k,t). \tag{68}$$

Thus the slow portion of the memory kernel is gradually incorporated through the iteration procedure.

A numerical solution of $\mathbf{F}^s(k,t)$ can be obtained in a similar fashion. Notice that it is required to solve the equations for $\mathbf{F}(k,t)$ and $\mathbf{F}^s(k,t)$ *simultaneously*, since the former enters the equation for the latter through Eq. (44), while the latter appears in the equation for the former through the auxiliary function [Eq. (35)]. Having obtained converged results for $\mathbf{F}(k,t)$, $\mathbf{F}^s(k,t)$ and their memory kernels, velocity correlation functions and the diffusion-coefficient matrix can be calculated from Eqs. (55) and (59). The site-site structure factors and direct correlation functions, which are required as input in our theory for dynamics, are obtained from ex-RISM integral equation theory [22,23].

IV. RESULTS AND DISCUSSION

A. System description and static structure factors

In this paper, we consider the same liquid model as paper I. This liquid consists of rigid diatomic molecules depicted in Fig. 1, with constituent atoms A and B of masses $m_A=36\ \mathrm{g\,mol^{-1}}$ and $m_B=4\ \mathrm{g\,mol^{-1}}$ separated from each other by a fixed distance of $l_{AB}=2.0$ Å. Atoms A and B carry partial charges $q_A=-0.25e$ and $q_B=+0.25e$, respectively, and the resultant dipole moment is 2.4 D. The Lennard-Jones parameters are $\sigma_A=4.0$ Å and $\epsilon_A/k_B=200$ K for atom A, and $\sigma_B=2.0$ Å and $\epsilon_B/k_B=100$ K for atom B. It should be remembered throughout this section that atom A is larger and heavier than atom B. The number density is 0.012 molecules $\mathrm{Å}^{-3}$, and the temperature is 250 K.

To see a consequence of the inclusion of a slow contribution in the memory kernels representing the correlated collisional effects, we have carried out two sets of calculations. The first set of calculations was performed by letting $\mathbf{K}(k,t)=\mathbf{K}_{\mathrm{fast}}(k,t)$ and $\mathbf{K}^s(k,t)=\mathbf{K}^s_{\mathrm{fast}}(k,t)$ (i.e., the memory kernels consist of the fast portion only), and the results so obtained will be referred to as FAST results. Another set of calculations have been done by incorporating the slow portion in the memory kernels as well, Eqs. (28) and (39), and the results based on this set of calculations will be called FULL results. It is then possible to deduce the consequence of the inclusion of the slow portion in the memory kernels by comparing FAST and FULL results. FAST and FULL results together will also be referred to as the theoretical results.

To test the accuracy of our theory, we have also carried out a molecular dynamics (MD) simulation of a system composed of 216 molecules confined in a cubic box of length $L=26.207$ Å at the chosen thermodynamic point using the program IMPACT [29]. The interaction potential was calculated with periodic boundary conditions and truncated at $L/2$. The temperature was controlled according to Berendsen

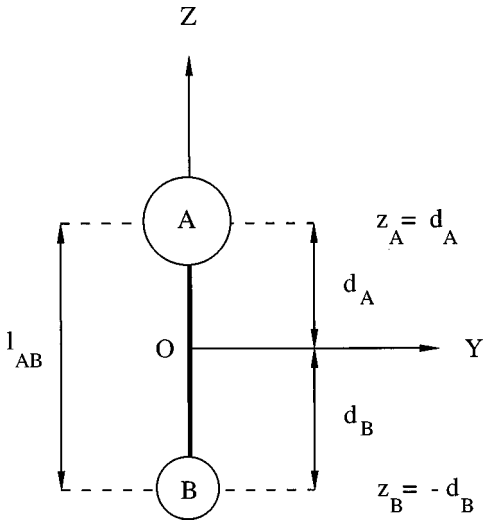

FIG. 1. Schematic representation of a diatomic molecule, consisting of atoms A and B, in the body-fixed molecular frame where the origin is taken to be the center of mass and the z axis is along the principal axis of the molecule. z_A and z_B denote the z coordinates of atoms A and B, respectively, and l_{AB} the bond length of the molecule.

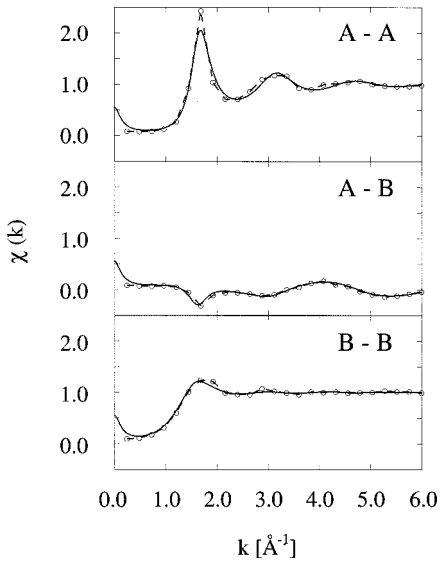

FIG. 2. The site-site static structure factors of the diatomic molecule, defined in Eq. (7). Solid lines denote the results calculated from ex-RISM, while circles represent MD results. The dashed lines are to guide the eyes.

et al.'s ''coupling to a heat bath'' method [30]. These technical aspects of the simulation may be too primitive to make the simulation results conclusive. However, we believe that the qualitative nature of the simulation results will not be changed if we employ more sophisticated techniques for the simulation such as the Ewald sum and the Nosé thermostat [31]. The simulation consists of 200 000 steps, with a time step of 1.0×10^{-15} s. The wave vector k for time-correlation functions and their spectra is chosen to be of the form $k=2\pi/L(n,0,0)$ with $n=1,\ldots,10$, and the average over the three independent components is performed in order to improve the statistics. The minimum accessible wave vector from MD simulation is $k_{\min}=0.2398$ Å^{-1}. The results obtained from the simulation will be called MD results. To facilitate the comparison, FAST and FULL results will also be reported at those wave vectors where MD results are available.

Figure 2 gives the site-site static structure factors calculated from ex-RISM (solid lines) and from MD simulation (circles). It is seen from the figure that ex-RISM results are quantitatively in good agreement with MD results, except for the peak height of $\chi_{AA}(k)$ [32]. Thus, the discrepancy, if found, between our theoretical results and MD results to be presented below can be attributed to a large extent to the approximations made in our theory for dynamics, which are summarized below Eq. (33) and Sec. III A.

For later convenience, we define here two quantities in terms of the site-site static structure factors which turn out to characterize collective excitations in molecular liquids in the small wave-vector regime (see below). The first one is defined by

$$\chi(0)\equiv\chi_{AA}(0)=\chi_{AB}(0)=\chi_{BB}(0), \tag{69}$$

where we have noticed that all the site-site structure factors coincide in the $k\to0$ limit [33]. It is well known that $\chi(0)$ is related to the isothermal compressibility of the fluid. We define the second one in terms of the second moment of the site-site static structure factors by

$$\chi''(0)\equiv\chi''_{AA}(0)+X''_{BB}(0)-2\chi''_{AB}(0), \tag{70}$$

with

$$\chi''_{\alpha\beta}(0)=\lim_{k\to0} d^2\chi_{\alpha\beta}(k)/dk^2. \tag{71}$$

$\chi''(0)$ is related to the dielectric constant ϵ of the fluid [34,35], and for our model liquid, it holds that

$$\chi''(0)=\frac{1}{2\pi\beta\rho q_A^2}\left(1-\frac{1}{\epsilon}\right). \tag{72}$$

B. Longitudinal current spectra

In this subsection, we study collective density fluctuations in the molecular fluid on the basis of the GLE [Eq. (26)]. As in our earlier study in paper I, this will be done by analyzing the longitudinal current spectra $\mathbf{C}_L(k,\omega)$ rather than the dynamic structure factors $\mathbf{S}(k,\omega)$. Since the fluctuations in density are intimately related to those in the longitudinal current due to the continuity equation [Eq. (3)], the physical information contained in these two quantities are essentially the same [see Eq. (14)], and the peak positions in the longitudinal current spectra in the small-k region can naturally be assigned to collective excitation modes in the fluid [10].

According to Eq. (26), the collective density fluctuations are characterized by two basic quantities $\langle\boldsymbol{\omega}_k^2\rangle$ and $\mathbf{K}(k,t)$. If we neglect the latter (the nondamping approximation), there would be resonances at frequencies determined by $\langle\boldsymbol{\omega}_k^2\rangle$, which depends on the inertia parameters contained in $\mathbf{J}(k)$ (whose explicit expression was presented in paper I) and on the static structure factors of the fluid [see Eq. (27)].

Detailed analysis of $\langle\boldsymbol{\omega}_k^2\rangle$ of the liquid under study was carried out in paper I based on the matrix-diagonalized procedure. It was shown that there are two different eigenmodes in this liquid which are collective in the small-k region: the acoustic and optical modes, which arise essentially from the translational and rotational (librational) motions of constituent molecules. (Equivalently, it can be said that these two modes originate from the mass-density and charge-density fluctuations of molecules, respectively.) Their resonance frequencies within the nondamping approximation in the $k\to0$ limit are given by [1]

$$\omega_{\mathrm{acou}}^2(k\to0)=\frac{k_BT}{M\chi(0)}k^2, \tag{73}$$

$$\omega_{\mathrm{opti}}^2(k\to0)=\frac{4k_BT}{3I\chi''(0)}l_{AB}^2, \tag{74}$$

where M and I are the total mass and the principal moment of inertia of the molecule, respectively. It is important to notice that $\omega_{\mathrm{opti}}(k)$ does not vanish in the $k\to0$ limit. (The term ''optical'' comes from this fact.) Thus, the analysis of $\langle\boldsymbol{\omega}_k^2\rangle$ reveals the existence of two distinct resonances in the collective density fluctuations, the lower-frequency acoustic mode and the higher-frequency optical one.

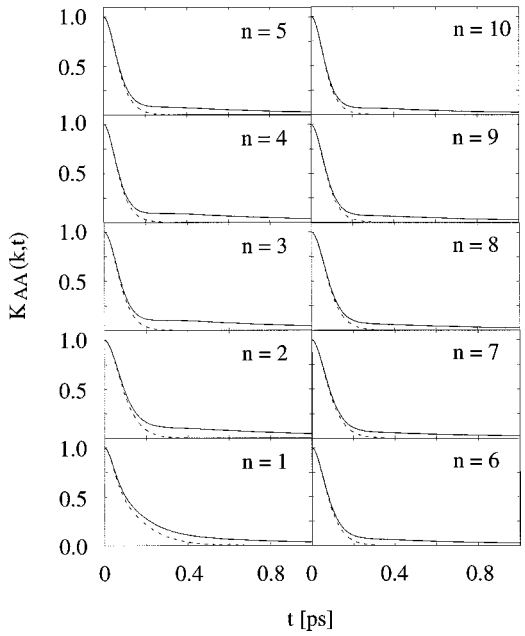

FIG. 3. Normalized memory functions of atom A, $K_{AA}(k,t)$, for $k=2\pi n/L$ with $n=1,\ldots,10$. Solid and dashed lines denote FAST and FULL results, respectively.

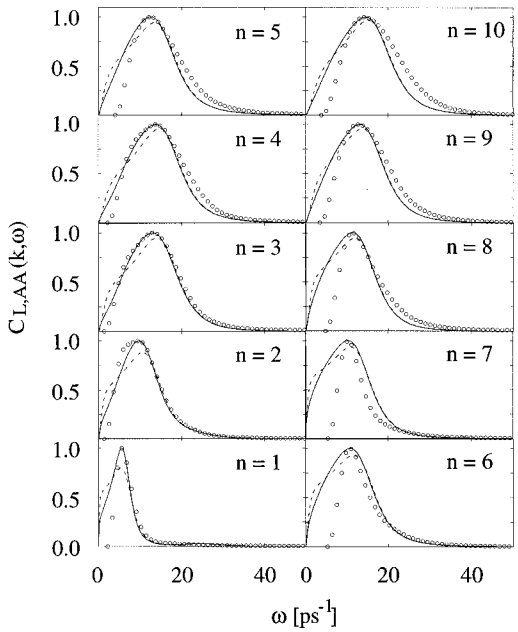

FIG. 5. The longitudinal current spectra of atom A, $C_{L,AA}(k,\omega)$, as a function of ω for $k=2\pi n/L$ with $n=1,\ldots,10$, in arbitrary units. Solid and dashed lines denote FAST and FULL results, respectively, and circles represent MD results. These results are scaled and shifted appropriately (see the text).

These resonances determined by $\langle \boldsymbol{\omega}_k^2 \rangle$ are shifted and damped by the memory kernel $\mathbf{K}(k,t)$. Figures 3 and 4 report the theoretical results for $K_{AA}(k,t)$ and $K_{BB}(k,t)$, respectively. In these figures, FAST and FULL results are denoted as dashed and solid lines, respectively, and the slow portion of the memory functions shows up as the difference of them.

The first noteworthy features from Figs. 3 and 4 are that the slow contribution in $K_{AA}(k,t)$ is larger than that in $K_{BB}(k,t)$, and that the overall decay of $K_{AA}(k,t)$ is slower compared to $K_{BB}(k,t)$. These features are reasonable considering that the larger atom A suffers more collisional effects compared to the smaller atom B, and that the heavier atom A is primarily responsible for the slower translational motion of the molecule, whereas the faster rotational (or librational) motion mainly originates from the motion of the lighter atom B. Another feature we found from a visual inspection of figures of the memory kernel in the larger wave vectors (not shown) is that the contribution from the slow portion decreases as the wave vector is increased. This can be understood by noting that the dynamics is more determined by short-duration events in the large-k regime (i.e., in the short-distance scale).

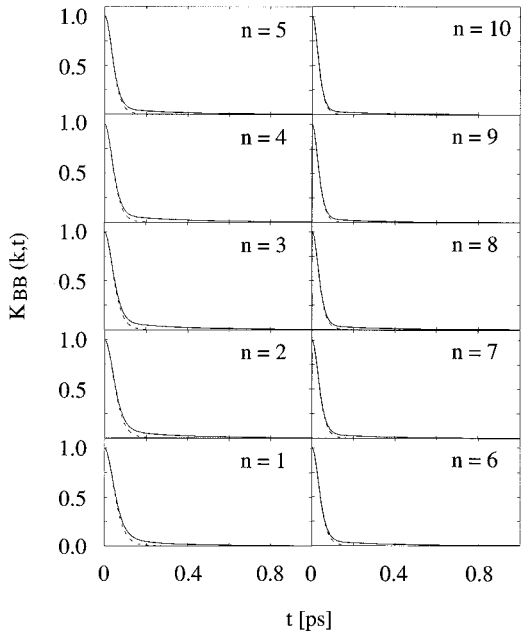

FIG. 4. Normalized memory functions of atom B, $K_{BB}(k,t)$, for $k=2\pi n/L$ with $n=1,\ldots,10$. Solid and dashed lines denote FAST and FULL results, respectively.

Now let us analyze the theoretical results for the longitudinal current spectra obtained by solving the GLE [Eq. (26)], that incorporates the damping effect from the memory kernel. The longitudinal current spectra for atoms A and B, $C_{L,AA}(k\omega)$ and $C_{L,BB}(k\omega)$, are presented in Figs. 5 and 6, respectively. In these figures, FAST and FULL results are denoted as dashed and solid lines, respectively, and their intensities are scaled by the same factor such that the areas under FAST and FULL results are equal at each wave vector.

Two different excitation peaks can be observed from Figs. 5 and 6 which are predicted from the analysis of $\langle \boldsymbol{\omega}_k^2 \rangle$, and are damped due to the presence of $\mathbf{K}(k,t)$. The lower-frequency peaks are those of the acoustic mode, which show up mainly in $C_{L,AA}(k,\omega)$, since the larger and heavier atom A is primarily responsible for the translational motion of the molecule. The lower-frequency peaks are also observable in Fig. 6 at small wave vectors (especially at $n=1$) since, of course, atom B also participates in the translational motion of the molecule. However, $C_{L,BB}(k,\omega)$ is dominated by the contribution by the contribution from the higher-frequency optical mode since the smaller and lighter atom B is mainly

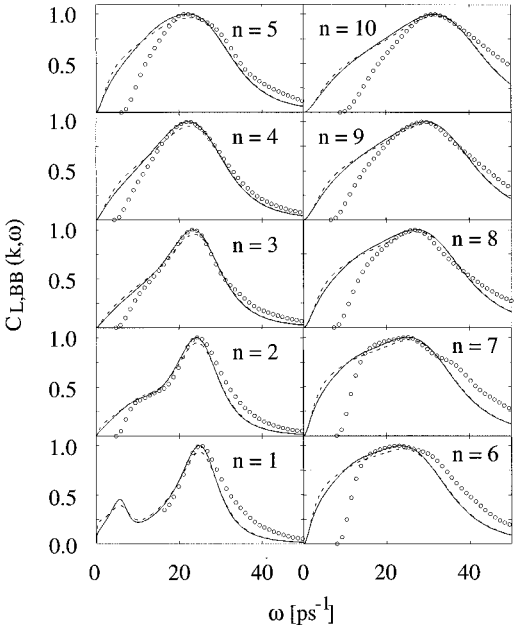

FIG. 6. The longitudinal current spectra of atom B, $C_{L,BB}(k,\omega)$, as a function of ω for $k=2\pi n/L$ with $n=1,\ldots,10$, in arbitrary units. Solid and dashed lines denote FAST and FULL results, respectively, and circles represent MD results. These results are scaled and shifted appropriately (see the text).

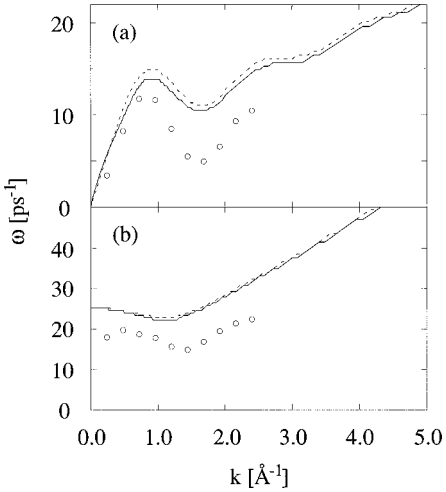

FIG. 7. The dispersion relation of the (a) acoustic and (b) optical modes as evaluated from the peak positions in the longitudinal current spectra. Solid and dashed lines denote FAST and FULL results, respectively, and circles represent MD results.

responsible for the orientational motion of the molecule.

Let us investigate how the inclusion of the slow contribution in the memory kernel affects the excitation profiles by comparing FAST and FULL results. From the results in Fig. 3, one expects a non-negligible effect from the slow contribution on the acoustic-mode excitation profiles, especially in the small-k region. We see from Fig. 5 that FULL results (solid lines) differ from the corresponding FAST results (dashed lines) especially in the lower-frequency parts of the acoustic-mode resonances: the difference reflects the effect of the inclusion of the slow portion in the memory kernel. This trend, however, decreases as the wave vector is increased, since the dynamics in the large-k regime is mainly accounted for by the short-duration events. On the other hand, FAST and FULL results for the optical-mode excitation profiles presented in Fig. 6 do not differ so significantly. This feature is expected from the results in Fig. 4, and by noting that the optical mode originates from the faster processes (librational motions) in the liquid.

The wave-vector dependence of low and high peak frequencies (dispersion relation) of the longitudinal current spectra are shown in Figs. 7(a) and 7(b), respectively. In these figures, FAST and FULL results are again denoted by dashed and solid lines, respectively. The dispersion behavior of the acoustic and optical modes shows the same trend as we discussed in paper I. It is seen from Figs. 7(a) and 7(b) that the peak frequencies are rather well reproduced even by taking into account only the fast portion of the memory kernel. Thus the effect of the inclusion of the slow contribution in the memory kernel mainly shows up in the spectral width of the lower-frequency acoustic mode.

Finally, we compare the theoretical results with MD results. The longitudinal current spectra obtained from the MD simulation are presented as circles in Figs. 5 and 6. To facilitate the comparison with the theoretical results, MD results are scaled vertically and shifted horizontally such that their peak positions and intensities coincide with FULL results. The actual peak frequencies obtained from MD simulations are separately reported as circles in Figs. 7(a) and 7(b).

Concerning the spectral width of the acoustic-mode excitation profiles presented in Fig. 5, FULL results show better agreement with MD results, and the inclusion of the slow contribution in the memory kernel actually improves the theoretical results. However, the theoretical results near the peak position of $\chi_{AA}(k)$ (i.e., $n=6,7$, and 8) deviate rather significantly from MD results. The disagreement is partly due to the equilibrium structure functions used in our theoretical calculations: as we have seen in Fig. 2, the peak height of $\chi_{AA}(k)$ obtained by ex-RISM is not in good agreement with that obtained from MD simulation. This is also reflected in the acoustic-mode dispersion relation near $n=7$ presented in Fig. 7(a). Another reason for the disagreement seems to lie in our approximate treatment of the fast portion of the memory kernel (see Sec. III A), since the disagreement is significant at the level of FAST results.

The theoretical results for the optical-mode excitation profiles are in fair agreement with MD results in the small-k region, but the agreement becomes worse at larger wave vectors. We presume that a primary reason for the discrepancy also lies in our approximate treatment of the fast portion of the memory kernel (see Sec. III A), since the motion of atom B is mainly responsible for the optical mode and since $K_{BB}(k,t)$ is largely determined by its fast portion (see Fig. 4). Thus it is clear that Eq. (66) may be a rather rough approximation for the fast portion of the memory kernel, and the improvement of the treatment should be investigated in the future.

As can be seen from Figs. 7(a) and 7(b), compared to MD results, our theoretical results reproduce the correct wave-vector dependence of the peak frequencies both of the acoustic and optical modes, although they are not in quantitative agreement. It is also seen from these figures that the inclusion of the slow contribution in the memory kernel seems to

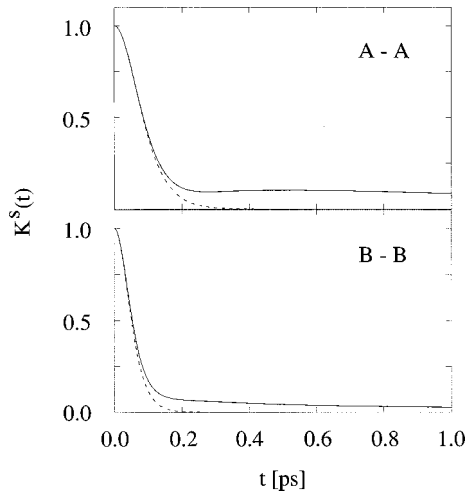

FIG. 8. Normalized memory functions of atoms A and B, $K_{AA}(t)$ and $K_{\mathrm{BB}}(t)$, for the velocity correlation functions. Solid and dashed lines denote FAST and FULL results, respectively.

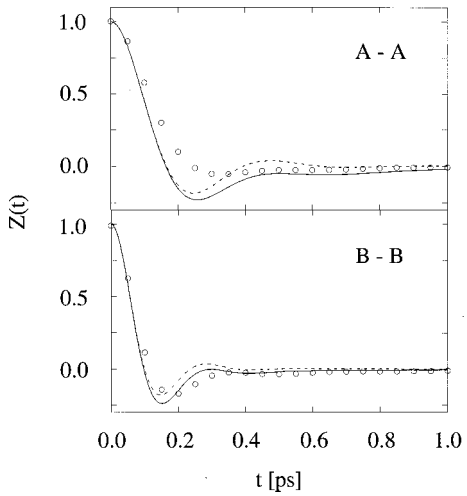

FIG. 9. Normalized velocity autocorrelation functions of atoms A and B, $Z_{AA}(t)$ and $Z_{BB}(t)$. Solid and dashed lines denote FAST and FULL results, respectively, and circles represent MD results.

improve the theoretical results toward MD results.

The MD result for the optical mode at the lowest wave vector (i.e., $n=1$) in Fig. 7(b) is seen to behave differently from the theoretical results. However, we have confirmed that the peak frequency of the optical mode at the lowest wave vector depends largely on the cutoff length used in MD simulation for the interaction potential, and the exceptional behavior seems to be an artifact caused by the cutoff. This indirectly indicates the collective nature of the optical-mode resonances in the small-k region. (The collective and single-particle nature of the excitation modes were already discussed in paper I, and it is possible to discuss the same matter based on the present work. We have verified that the conclusion does not change from paper I, and such a discussion will be omitted here for brevity.)

C. Velocity autocorrelation functions and diffusion coefficients

We next turn our attention to single-particle dynamics. Specifically, here we analyze velocity autocorrelation functions and diffusion coefficients of the molecular liquid.

Figure 8 reports the normalized memory functions for the velocity correlation functions $\mathbf{K}(t)$ defined in Eq. (55), for atoms A and B: solid and dashed lines denote FAST and FULL results, respectively. It is seen by comparing FAST and FULL results that the contribution from the slow portion is larger for $K_{AA}(t)$ compared to $K_{BB}(t)$, which is the same trend as we have observed in Figs. 3 and 4.

The normalized velocity autocorrelation functions are presented in Fig. 9 which is obtained by solving Eq. (55), and their spectra are reported in Fig. 10, along with MD results. In these figures, again, solid and dashed lines denote FAST and FULL results, respectively, and circles represent MD results. In Fig. 10, FAST and FULL results are scaled by the same factor such that the areas under them are equal, while MD results are scaled so that their peak intensities coincide with those of FULL results. (No horizontal shift of MD spectra is attempted in Fig. 10.)

From Figs. 9 and 10, one sees that, although the overall features are well reproduced by our theory, the theoretical results for the velocity autocorrelation function and its spectrum for atom A are not in good agreement with MD results, even with the inclusion of the slow portion of the memory kernel. On the other hand, the theoretical results for atom B are in fair agreement with MD results, and that the inclusion of the slow contribution in the memory kernel is seen to improve the theoretical results.

We next discuss the diffusion coefficients of our model liquid. To this end, we take the same approach as that employed in paper I in analyzing $\langle \boldsymbol{\omega}_k^s \rangle$, i.e., the matrix-diagonalization procedure.

The k-dependent diffusion-coefficient matrix is calculated from Eq. (59), and its eigenvalues are reported in Fig. 11(a). (For brevity, only FULL results are reported in Fig. 11.) Figure 11(a) clearly shows that there are two eigenvalues of $\mathbf{D}(k)$ which behave in the small-k regime as we anticipated in Sec. II E [see Eq. (63)]: one of the eigenvalues behaves as k^2D^T in the small-k regime [solid line in Fig. 11(a)], while the other converges into a finite value (D^R) in the $k\rightarrow 0$ limit

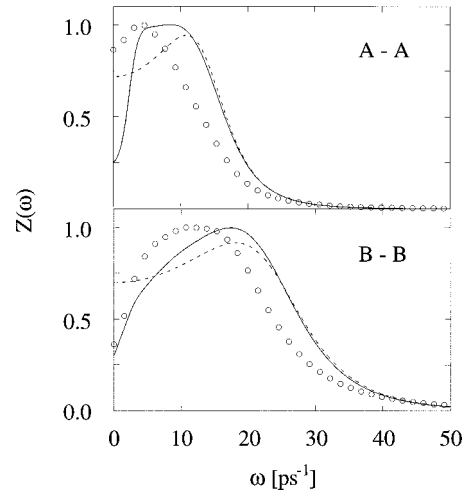

FIG. 10. Spectra of the velocity autocorrelation functions of atoms A and B, $Z_{AA}(\omega)$ and $Z_{BB}(\omega)$. Solid and dashed lines denote FAST and FULL results, respectively, and circles represent MD results. These results are scaled (but not shifted) appropriately (see the text).

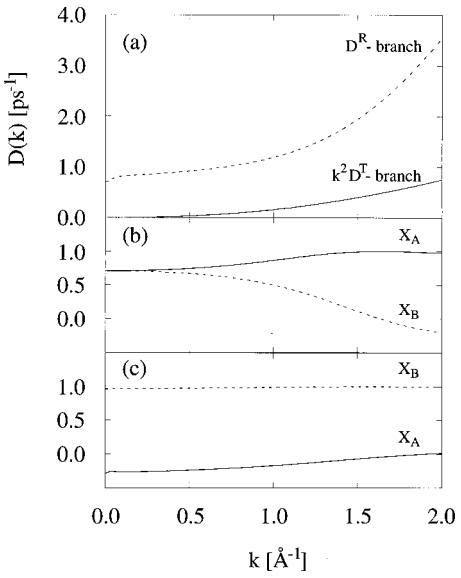

FIG. 11. (a) Diffusion coefficients as evaluated by diagonalizing the diffusion-coefficient matrix $\mathbf{D}(k)$. Only FULL results are reported. Solid and dashed lines denote k^2D^T and D^R branches of the eigenvalues of $\mathbf{D}(k)$, respectively. (b) x_A (solid line) and x_B (dashed line) defined in the text corresponding to the k^2D^T branch. (c) x_A (solid line) and x_B (dashed line) corresponding to the D^R branch. x_A and x_B are normalized such that $x_A^2+x_B^2=1$.

[dashed line in Fig. 11(a)]. As mentioned in Sec. II E, the former can be regarded as the translational diffusion coefficient, and the latter the rotational diffusion coefficient.

To further confirm that D^T and D^R actually reflect the translational and rotational motions of the molecule, respectively, we investigate how the motion of each atom in the molecule contributes to D^T and D^R. The contributions from each atom to the translational and rotational diffusion coefficients can be extracted in the following way. Diagonalizing the matrix $\mathbf{D}(k)$ corresponds to changing the description of the system from one in terms of the densities of each atom $\delta\rho_A(\mathbf{k})$ and $\delta\rho_B(\mathbf{k})$ to one in terms of their linear combination,

$$x_A(k)\,\delta\rho_A(\mathbf{k})+x_B(k)\,\delta\rho_B(\mathbf{k}), \tag{75}$$

where $x_A(k)$ and $x_B(k)$ are the components of the eigenvector corresponding to each eigenvalue of $\mathbf{D}(k)$.

Figure 11(b) reports $x_A(k)$ and $x_B(k)$ corresponding to the k^2D^T branch, normalized such that $x_A^2(k)+x_B^2(k)=1$. It is seen from the figure that $x_A(k)=x_B(k)$ holds in the $k\rightarrow 0$ limit. This reveals that both atoms in the molecule equally contribute to D^T, and thus verifies that D^T originates from the center-of-mass translational motion of the molecule.

Figure 11(c) presents $x_A(k)$ and $x_B(k)$ corresponding to the D^R branch. Note from the figure that $x_A(k)$ and $x_B(k)$ in the $k\rightarrow 0$ limit are opposite in sign; thus atoms A and B contribute to D^R in an out-of-phase fashion in terms of Eq. (75). (Suppose that a molecule in Fig. 1 rotates around the x axis. Then the z component coordinate of atom A decreases while that of atom B increases. The out-of-phase fashion mentioned above implies this kind of motion, i.e., rotation. Also see the discussion concerning the matrix $\langle\boldsymbol{\omega}_k^2\rangle$ presented in paper I.) It should be also noted that the magnitude of $x_B(k)$ is larger than that of $x_A(k)$, indicating that the lighter atom B is more responsible in determining D^R. These facts confirm that D^R indeed reflects the rotational motion of the molecule.

TABLE I. The theoretical and MD results for the translational and rotational diffusion coefficients. The theoretical results are obtained by taking the $k\rightarrow 0$ limit of the eigenvalues of $\mathbf{D}(k)$ (see the text).

	FAST	FULL	MD
D^T (Å^2 ps^{-1})	0.367	0.091	0.501
D^R(ps^{-1})	1.325	0.712	0.744

Numerical FAST and FULL results for D^T and D^R are reported in Table I. FULL results for diffusion coefficients are small compared to FAST results, since the inclusion of the slow contribution in the memory kernel increases the translational as well as rotational frictions ''felt'' by the tagged molecule [see Eq. (57)].

MD results for D^T and D^R are also calculated from trajectories using the standard formulas [11]

$$D^T=\tfrac{1}{3}\int_0^\infty dt\langle\mathbf{v}^C(0)\cdot\mathbf{v}^C(t)\rangle, \tag{76}$$

$$D^R=\tfrac{1}{2}\int_0^\infty dt\langle\boldsymbol{\omega}(0)\cdot\boldsymbol{\omega}(t)\rangle, \tag{77}$$

where $\mathbf{v}^C(t)$ and $\boldsymbol{\omega}(t)$ denote the center-of-mass velocity and the angular velocity of a molecule, respectively, and are given in Table I. It is seen from the table that the FULL result for D^R is in good agreement with the corresponding MD result, while that for D^T is not so good. This is in accord with our observation in Figs. 9 and 10, since the velocity autocorrelation function of the lighter atom B reflects the orientational motion of the molecule, for which the theoretical results are found to be in good agreement with MD results.

V. CONCLUDING REMARKS

In the present paper, numerical results were presented for longitudinal current spectra, velocity autocorrelation functions, and diffusion coefficients of a model diatomic liquid using the theory developed in paper II. The theory is based on the interaction-site model for molecular liquids, the projection-operator formalism of Zwanzig and Mori, and the mode-coupling theory. By comparing FAST and FULL results, the effect of the inclusion of the slow contribution in the memory kernels on the aforementioned dynamical quantities was discussed. The molecular dynamics simulation of the same system was also performed to test the accuracy of the theory, and the theoretical results were found to be in fair agreement with the simulation results.

Finally, one should note the following important feature which our theory for dynamics based on the interaction-site model (ISM) provides. That is, although our theory based on

the ISM stands on the atomic viewpoint (more precisely, the correlated-atom viewpoint due to the presence of chemical bonds), and the resulting dynamical correlation functions are the site-site ones, it is possible to extract such physics of molecular liquids as the translational and rotational motions from the site-site correlation functions. For instance, the site-site longitudinal current spectra can be reasonably interpreted in terms of the acoustic and optical modes arising, respectively, from the translational and rotational motions of the molecules. The latter viewpoint was employed in Ref. [36] in the problem of the ionic friction in a polar liquid, and it has been demonstrated that contributions from the translational and rotational motions of surrounding solvent molecules on an ionic friction can be separately discussed by taking appropriate linear combinations of the site-site space-time density correlation functions. As another example, as showed in Sec. IV C, although a bare application of Eq. (59) to a polyatomic fluid results in a diffusion-coefficient matrix whose elements represent the correlated atomic diffusion, it is possible to extract the translational and rotational diffusion coefficients of the molecule by diagonalizing the matrix $\mathbf{D}(k)$. It is worth noting that, to our knowledge, this is the first molecular theory to *predict* the rotational diffusion coefficient from first principles.

This feature in our theory is in contrast to another method of describing the dynamics of polyatomic fluids, i.e., the one based on rotational invariant expansions [33,37,38] which can deal explicitly with reorientational motion as well as center-of-mass-motion-dependent quantities. However, the method based on rotational invariant expansions becomes increasingly difficult as the asphericity of a molecule becomes larger, since the convergence of the invariant expansion is slow. Our theory based on the ISM, on the other hand, does not suffer from this problem, and is superior to the other in applying to a system consisting of complicated molecules. Thus our theory is not only capable of treating the general class of polyatomic fluids without too much difficulty, but can also be used to extract the important physics of molecular liquids, and paves a way toward a theory for dynamical processes in polyatomic fluids.

ACKNOWLEDGMENTS

S.-H.C. gratefully acknowledges financial support from the Japan Society for the Promotion of Science for Young Scientists. This work was supported by the Joint Studies Program of the Institute for Molecular Science.

[1] S.-H. Chong and F. Hirata, Phys. Rev. E **57**, 1691 (1998).
[2] S.-H. Chong and F. Hirata, Phys. Rev. E (to be published).
[3] R. Zwanzig, in *Lectures in Theoretical Physics*, edited by W. E. Britton, B. W. Downs, and J. Downs (Wiley Interscience, New York, 1961), Vol. III, p. 135.
[4] H. Mori, Prog. Theor. Phys. **33**, 423 (1965).
[5] H. Mori, Prog. Theor. Phys. **34**, 399 (1965).
[6] D. Chandler and H. C. Andersen, J. Chem. Phys. **57**, 1930 (1972).
[7] D. Chandler, in *The Liquid State of Matter*, edited by E. Montroll and J. L. Lebowitz (North-Holland, Amsterdam, 1982).
[8] S. W. Lovesey, J. Phys. C **4**, 3057 (1971).
[9] J. R. D. Copley and S. W. Lovesey, Rep. Prog. Phys. **38**, 461 (1975).
[10] J. P. Boon and S. Yip, *Molecular Hydrodynamics* (McGraw-Hill, New York, 1980).
[11] J.-P. Hansen and I. R. McDonald, *Theory of Simple Liquids*, 2nd ed. (Academic, London, 1990).
[12] U. Balucani and M. Zoppi, *Dynamics of the Liquid State* (Oxford University Press, New York, 1994).
[13] G. F. Mazenko, Phys. Rev. A **7**, 209 (1973).
[14] G. F. Mazenko, Phys. Rev. A **9**, 360 (1974).
[15] W. Götze and M Lücke, Phys. Rev. A **11**, 2173 (1975).
[16] T. Munakata and A. Igarashi, Prog. Theor. Phys. **58**, 1345 (1977).
[17] T. Munakata and A. Igarashi, Prog. Theor. Phys. **60**, 45 (1978).
[18] J. Bosse, W. Götze, and M Lücke, Phys. Rev. A **17**, 434 (1978).
[19] J. Bosse, W. Götze, and M Lücke, Phys. Rev. A **17**, 447 (1978).
[20] L. Sjögren, Phys. Rev. A **22**, 2866 (1980).
[21] L. Sjögren, Phys. Rev. A **22**, 2883 (1980).
[22] F. Hirata and P. J. Rossky, Chem. Phys. Lett. **83**, 329 (1981).
[23] F. Hirata, B. M. Pettitt, and P. J. Rossky, J. Chem. Phys. **77**, 509 (1982).
[24] M. A. Ricci, D. Rocca, G. Ruocco, and R. Vallauri, Phys. Rev. A **40**, 7226 (1989).
[25] H. Resat, F. O. Raineri, and H. L. Friedman, J. Chem. Phys. **97**, 2618 (1992).
[26] H. W. Jackson and E. Feenberg, Rev. Mod. Phys. **34**, 686 (1962).
[27] J. Bosse and M. Henel, Ber. Bunsenges. Phys. Chem. **95**, 1007 (1991).
[28] F. Hirata, J. Chem. Phys. **96**, 4619 (1992).
[29] D. B. Kitchen, F. Hirata, J. D. Westbrook, R. M. Levy, D. Kofke, and M. Yarmush, J. Comput. Chem. **11**, 1169 (1990).
[30] H. J. C. Berendsen, J. P. M. Postma, W. F. Van Gunsteren, A. Di Nola, and J. R. Haak, J. Chem. Phys. **81**, 3684 (1984).
[31] M. P. Allen and D. J. Tildesley, *Computer Simulation of Liquids* (Oxford University Press, New York, 1987).
[32] There is another problem in ex-RISM on which our theory is based, namely, it can only give the ''ideal gas'' result for the static dielectric constant ϵ. [See, for example, D. E. Sullivan and C. G. Gray, Mol. Phys. **42**, 443 (1981).] However, we believe that the defect in ex-RISM does not affect the qualitative nature of the results in the present paper very significantly. For example, substituting Eq. (72) into Eq. (74) gives the dependence of $\omega_{\mathrm{opti}}(0)$ on the dielectric constant as $\omega_{\mathrm{opti}}(0) \propto (1-1/\epsilon)^{-1/2}$. Thus the effect from the defect in ex-RISM on $\omega_{\mathrm{opti}}(0)$ is small provided that $\epsilon \gg 1$ holds (ex-RISM gives $\epsilon = 9.40$ for our model liquid, which can be regarded as the lower limit of the true value). Nevertheless, it is an important and nontrivial problem to clarify how the defect in ex-RISM

affects, e.g., the wave-vector- and frequency-dependent dielectric function, and such a study will be deferred to a subsequent paper.

[33] C. G. Gray and K. E. Gubbins, *Theory of Molecular Fluids* (Oxford University Press, New York, 1984), Vol. I.

[34] M. Ohba and K. Arakawa J. Phys. Soc. Jpn. **50**, 743 (1981).

[35] F. O. Raineri, Y. Zhou, H. L. Friedman, and G. Stell, Chem. Phys. **152**, 201 (1991).

[36] S.-H. Chong and F. Hirata, J. Chem. Phys. **108**, 7339 (1998).

[37] D. Wei and G. N. Patey, J. Chem. Phys. **91**, 7113 (1989).

[38] D. Wei and G. N. Patey, J. Chem. Phys. **93**, 1399 (1990).